EDGE ARTICLE

Check for updates

Rational molecular design of multifunctional self-assembled monolayers for efficient hole selection and buried interface passivation in inverted perovskite solar cells†

Wenlin Jiang, [ID] ‡[abc] Ming Liu,‡[ac] Yanxun Li,[ac] Francis R. Lin [ID] [bc] and Alex K.-Y. Jen [ID] *[abcd]

Self-assembled monolayers (SAMs) have been widely employed as the bottom-contact hole-selective layer (HSL) in inverted perovskite solar cells (PSCs). Besides manipulating the electrical properties, molecularly engineering the SAM provides an opportunity to modulate the perovskite buried interface. Here, we successfully introduced Lewis-basic oxygen and sulfur heteroatoms through rational molecular design of asymmetric SAMs to obtain two novel multifunctional SAMs, **CbzBF** and **CbzBT**. Detailed characterization of single-crystal structures and device interfaces shows that enhanced packing, more effective ITO work function adjustment, and buried interface passivation were successfully achieved. Consequently, the champion PSC employing **CbzBT** showed an excellent power conversion efficiency (PCE) of 24.0% with a high fill factor of 84.41% and improved stability. This work demonstrates the feasibility of introducing defect-passivating heterocyclic groups into SAM molecules to help passivate the interfacial defects in PSCs. The insights gained from this molecular design strategy will accelerate the development of new multifunctional SAM HSLs for efficient PSCs.

Introduction

Organic–inorganic hybrid perovskite solar cells (PSCs) are considered to be one of the most exciting advancements in emerging photovoltaic technologies with a transcendent power conversion efficiency (PCE) currently reaching 26.1%.[1–3] Apart from engineering the perovskite compositions[4,5] and crystallization kinetics,[6–10] the key to further enhancing the performance and stability of PSCs lies in delicate engineering of the interfaces[11] between the perovskite absorber and contact interlayers.[12–15] In inverted PSCs, the use of ultrathin self-assembled monolayers (SAMs)[16–18] that can efficiently extract holes from perovskite to the anode as the hole-selective layer (HSL) has become increasingly popular.[19–21] Unlike PTAA or other conventional organic hole-transporting materials,[22] SAMs

offer new opportunities as an economic, scalable, and stable HSL in inverted PSCs due to the extremely low material consumption, simple fabrication, and feasibility of molecularly tailoring their chemical structures.[23,24]

SAM molecules based on functionalities of electron-rich conjugated backbones and phosphonic acid anchoring groups have been successfully adopted in high-performance inverted PSCs.[25–29] The electron-rich conjugated backbones should have a suitable highest occupied molecular orbital (HOMO) energy level and a suitable dipole moment pointing toward the ITO substrate for effectively tuning the substrate work function (WF).[18,30–32] Therefore, having the SAM HOMO energy level well-aligned with the perovskite valence band maximum (VBM) and controlling the molecular dipole orientation of the SAM with respect to the substrate are critical in designing new SAMs.[33,34] In addition, the structural tunability of the SAM backbone enables the introduction of functional groups that are capable of passivating defects of perovskites. This allows the integration of effective hole selectivity and passivation of buried interfaces in PSCs on one SAM molecule.

Asymmetric conjugated molecules usually have large molecular dipole moments,[35] but their dipole moments tend to cancel each other in the aggregated state by forming a quasi head-to-tail packing motif.[36] However, as SAM formation is templated by the substrate, the orientation of asymmetric SAM molecules can be fixed to avoid canceling the dipoles. Thus,

Department of Materials Science and Engineering, City University of Hong Kong, Kowloon 999077, Hong Kong. E-mail: alexjen@cityu.edu.hk

Department of Chemistry, City University of Hong Kong, Kowloon 999077, Hong Kong

Hong Kong Institute for Clean Energy, City University of Hong Kong, Kowloon 999077, Hong Kong

State Key Laboratory of Marine Pollution, City University of Hong Kong, Kowloon, 999077, Hong Kong

‡ These authors contributed equally to this work.

asymmetric conjugated molecules having strong molecular dipole moments can potentially improve the performance of SAM HSLs. Our recently reported carbazole-based asymmetric conjugation-extended SAM molecule **CbzPh**,[27] which was used as a HSL in inverted PSCs, exhibited superior performance to the symmetric carbazole-based SAM molecule 4PACz. This is attributed to the enhanced stacking and molecular dipole of the extended asymmetric conjugation, and their synergistic effect further alleviates the dipole elimination brought about by the disorderly oriented molecular dipole moments in the aggregated state. More recently, Wang *et al.* down-shifted the HOMO energy level of **CbzPh** through bromination,[37] making it suitable as a HSL for both wide-bandgap PSCs and organic solar cells, which also demonstrates the potential of SAM molecules based on an asymmetric conjugated backbone. Therefore, it is promising to further develop high-performance asymmetric SAM molecules through such a rational molecular design strategy.

Herein, we report two novel asymmetric SAM molecules designed through substituting the fused benzene ring on **CbzPh** with benzofuran and benzothiophene, obtaining **CbzBF** and **CbzBT**, respectively (Fig. 1). Their asymmetric structure ensures enhanced molecular dipole moments, and extended conjugation facilitates stronger intermolecular interactions to realize ordered and dense assembly of SAMs. Moreover, the introduction of lone-pair-rich, Lewis-basic heteroatoms of oxygen and sulfur can effectively passivate the uncoordinated Pb^{2+} at the buried interface in the PSC.[38] Based on the above-mentioned rational asymmetric molecular design, **CbzBF** and **CbzBT** have successfully achieved more efficient hole extraction and effective buried interface passivation, significantly improving the performance of the derived devices compared to those based on **CbzPh**. A champion PCE of 24.04% with improved device stability could be achieved by applying **CbzBT** as a HSL in an inverted PSC.

Results and discussion

The electrochemical properties of **CbzPh**, **CbzBF** and **CbzBT** were studied by cyclic voltammetry (CV) (Fig. S2†). The HOMO energy levels of **CbzPh**, **CbzBF** and **CbzBT** are estimated to be −5.48 eV, −5.46 eV, and −5.50 eV, respectively, which are nearly identical. This could facilitate a better cascade alignment between the SAM HOMO energy level and the VBM of the perovskite, ensuring efficient hole extraction from perovskite to the SAM. The lowest unoccupied molecular orbital (LUMO) energy levels of **CbzPh**, **CbzBF** and **CbzBT** were estimated to be −2.19 eV, −2.02 eV, and −2.10 eV, respectively, based on their optical bandgaps (Fig. S1†). These values are significantly higher than the conduction band minimum (CBM) of perovskites, thereby effectively blocking the electrons from reaching the anode. These results were further corroborated by density functional theory (DFT) computation (Fig. S3†), where the calculated HOMO energy levels for **CbzPh**, **CbzBF** and **CbzBT** were −5.49 eV, −5.50 eV and −5.54 eV, respectively, agreeing well with those obtained from the CV measurements.

The gas-phase molecular dipole moments were also calculated by DFT (Fig. S4†), among which **CbzBF** (2.48 D) and **CbzBT**
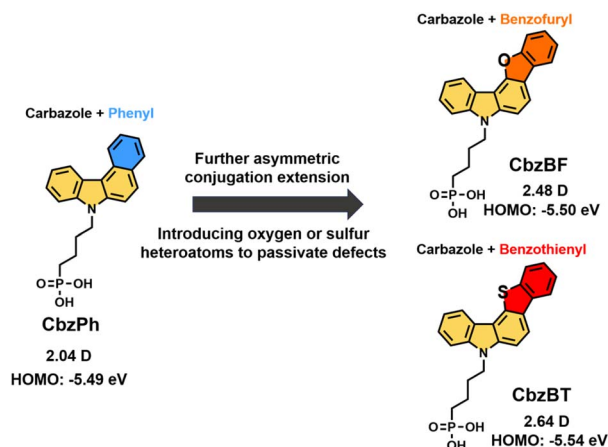

Fig. 1 Molecular structures, calculated dipole moments and HOMO energy levels of CbzPh, CbzBF, and CbzBT.

(2.64 D) both show larger dipole moments than **CbzPh** (2.04 D). It is notable that a larger molecular dipole pointing toward the substrate is favorable for down-shifting the ITO WF. As shown by UPS measurements (Fig. S5†), the WF of **CbzBF**- and **CbzBT**-modified ITO substrates is −5.08 eV and −5.27 eV, deeper than that modified with **CbzPh** (−4.92 eV). The surface morphology and potential of SAMs deposited on the ITO substrates were represented by Kelvin probe force microscopy (KPFM). As shown in Fig. S6,† there is no obvious change in the surface morphology of ultra-thin SAM-modified ITO and bare ITO, but their surface contact potential difference (CPD) is significantly improved compared with bare ITO. Compared to the CPD of −111.4 mV for bare ITO (Fig. S7†), significantly increased values of 206.1 mV, 363.2 mV and 669.6 mV were observed for **CbzPh**/ITO, **CbzBF**/ITO and **CbzBT**/ITO, respectively, confirming that **CbzBF** and **CbzBT** with larger molecular dipole moments can down-shift the ITO WF more effectively, which is consistent with the results of UPS. This should facilitate more efficient hole-extraction at the interface by minimizing the energy offset to achieve a higher fill factor (FF) and open-circuit voltage (V_{oc}) in the corresponding PSC.[26,27,33]

To gain deeper understanding into the molecular packing of **CbzPh**, **CbzBF**, and **CbzBT** in a condensed phase, single crystals suitable for XRD analysis of SAM π-scaffolds were obtained by slow evaporation from a solution in acetone. Although the packing of SAM π-scaffolds in their single crystals could differ from the packing pattern of substrate-supported SAM molecules, it could provide us valuable information for understanding and identifying the intrinsic intermolecular interactions in different π-extended carbazoles for establishing a comparison. This also excludes the interruption of strong intermolecular interactions from phosphonic acid anchoring groups, such as hydrogen bonding. The structures of π-scaffolds of **CbzPh**, **CbzBF**, and **CbzBT** are highly planar, and the twisting angles between the extended aryl group and the carbazole core are 4.27°, 2.29°, and 2.02°, respectively. For the π-scaffold of **CbzPh** (7*H*-benzo[*c*]carbazole), a large longitudinal slip of 5.48 Å indicates insufficient π–π interactions (Fig. 2a),

resulting in lack of close-contact interaction between two parallelly neighboring molecules. This may prevent **CbzPh** from forming an ordered assembly on the substrates. For the π-scaffold of **CbzBF** (5H-benzofuro[3,2-c]carbazole) and **CbzBT** (5H-benzo[4,5]thieno[3,2-c]carbazole), the relative slip distances between two adjacent parallel molecules are 5.33 Å and 5.29 Å, respectively (Fig. 2b and c). Moreover, the fused benzofuryl or benzothienyl moiety extends the conjugation length longer than phenyl, which enables stronger CH···π and π–π interactions between neighboring molecular π-planes. Such improved π–π interactions of **CbzBF** and **CbzBT** provide sufficient π–π overlap to facilitate the formation of more ordered and dense assemblies of the corresponding SAM molecules on the ITO substrate.

The SAMs were grown on ITO substrates by spin-coating their solutions in isopropanol (IPA), followed by annealing at 100 °C on a hot plate for 15 min, and the surface of the SAM-coated ITO substrate was rinsed with IPA to ensure removal of residual SAM molecules. To ensure the successful functionalization of **CbzPh**, **CbzBF** and **CbzBT** on ITO substrates, we characterized the surface atomic composition of these SAM-coated ITO substrates using high resolution X-ray photoelectron spectroscopy (HR-XPS). The characteristic signals of P 2p and S 2p electrons demonstrate the successful anchoring of **CbzPh**, **CbzBF**, and **CbzBT** on the ITO surface (Fig. S8–S11†). Moreover, a semi-quantitative analysis of the elemental contents by HR-XPS was conducted using previously reported methods[39,40] to identify the molecular density and regularity in SAMs. It was found that **CbzBF** and **CbzBT** have improved coverage factors[41] compared with **CbzPh** (Table S3†), indicating the formation of denser and more ordered monolayers of **CbzBF** and **CbzBT**. This can be attributed to the more pronounced π–π

interactions between their own molecules of **CbzBF** and **CbzBT**, as revealed by single crystals of their π-scaffolds. The formation of denser assemblies and more ordered packing of monolayers can synergize with the larger molecular dipoles to effectively tune the ITO WF, consistent with the UPS and KPFM measurements.

In inverted PSCs, the SAM-modified substrate plays a critical role in providing a crystallization template for the perovskite absorber, and a suitable non-wetting surface should facilitate the formation of a uniform and compact perovskite film.[42–44] To assess the surface wettability, contact angle measurements were performed on the SAM-modified ITO substrates. The contact angles of water droplets on **CbzPh**-, **CbzBF**- and **CbzBT**-modified substrates were measured to be 77.6°, 79.4°, and 86.6°, respectively (Fig. S13†), which can all serve as suitable non-wetting surfaces to facilitate perovskite crystallization.[27,43,45] Moreover, the introduction of heteroatoms usually improves the hydrophilicity of the surface, but we found that after the introduction of heteroatoms, the contact angles of **CbzBF** and **CbzBT** become even larger than that of **CbzPh**. This is attributed to the enhanced intermolecular interactions resulting from further extended conjugation that promotes the growth of **CbzBF** and **CbzBT** into denser monolayers,[46] just as the trend observed in single crystals, also echoing the HR-XPS results.

The SEM images of the perovskite films atop the **CbzPh**-, **CbzBF**- and **CbzBT**-modified substrates are shown in Fig. 3a. The morphology of perovskite films grown on different substrates showed significant differences, in which larger grain sizes were observed on the surface of **CbzBF**- and **CbzBT**-supported perovskites than that supported by **CbzPh** (Fig. 3a). The X-ray diffraction (XRD) of perovskite films deposited on different SAMs is shown in Fig. 3b. The perovskite phase does not exhibit any detectable peak shift or broadening, but they show different (110) crystal face diffraction intensity in the order of **CbzBT** > **CbzBF** > **CbzPh**, and different PbI_2 diffraction intensity in the order of **CbzBT** < **CbzBF** < **CbzPh** (Fig. S14†), indicating better perovskite film quality after introducing sulfur and oxygen heteroatoms to passivate the defects. The perovskite films with a higher PbI_2 content are known to reduce device stability owing to the formation of Pb^0, which can act as a non-radiative recombination center.[47] The improved film quality could also reduce the interfacial trap density and alleviate charge recombination to enhance the FF and V_{OC} of devices.[48,49]

The XPS spectra of the buried interface of perovskite films peeled off from the ITO/SAM substrate also confirmed the passivation effect of **CbzBF** and **CbzBT** on Pb^{2+}, because there was a shift in the Pb 4f peak of perovskite films spin-coated on ITO/**CbzBF** and ITO/**CbzBT** compared with those on ITO/**CbzPh** (Fig. S12†). The decrease in Pb^{2+} binding energy is due to the sharing of lone pair electrons by oxygen or sulfur atoms on **CbzBF** and **CbzBT** with Pb^{2+},[50,51] which reiterates our achieved buried interface passivation through rational SAM molecular structure design.

Based on these encouraging findings, **CbzPh**, **CbzBF**, and **CbzBT** SAMs were applied as HSLs for fabricating inverted PSCs to evaluate their effectiveness with a device configuration of ITO/SAM/perovskite/C$_{60}$/BCP/Ag (Fig. 4a). The reference device
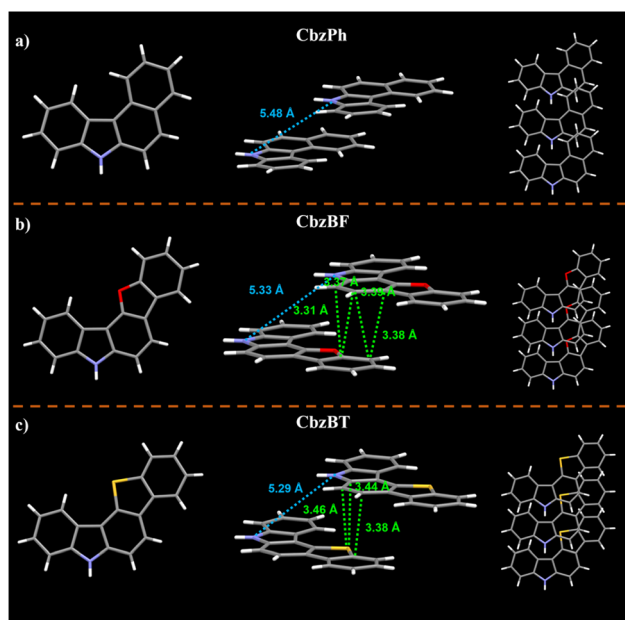

Fig. 2 The molecular packing patterns in single crystals of the π-scaffolds of (a) **CbzPh** (7H-benzo[c]carbazole), (b) **CbzBF** (5H-benzofuro[3,2-c]carbazole), and (c) **CbzBT** (5H-benzo[4,5]thieno[3,2-c]carbazole).
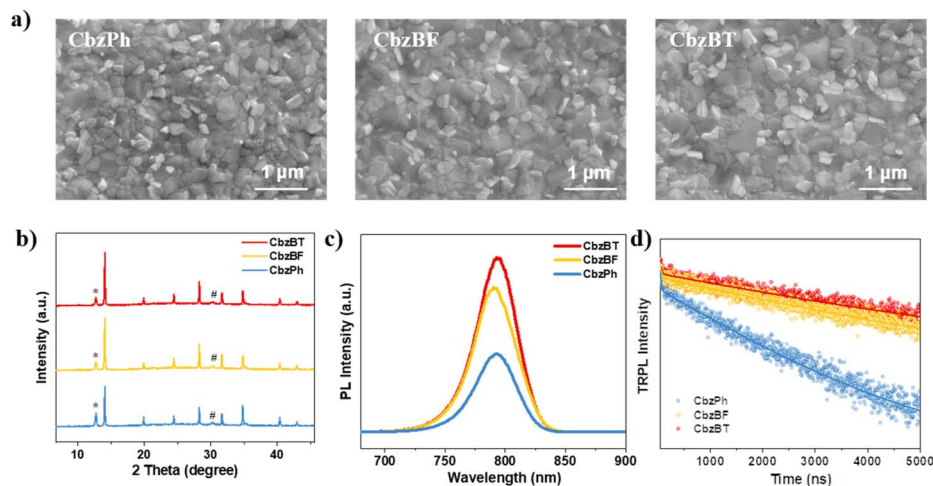
Fig. 3 (a) The SEM images, (b) XRD patterns (here * denotes the diffraction peak of PbI$_2$ and # denotes the diffraction peak of ITO), (c) PL spectra and (d) TRPL spectra (the direction of incident light comes from the perovskite side) of perovskite films deposited on **CbzPh**, **CbzBF** and **CbzBT** HSLs.

based on **CbzPh** showed an average PCE of 19.36% with a V_{oc} of 1.06 V, short-circuit current density (J_{sc}) of 23.58 mA cm^{-2}, and FF of 76.56% under 1-sun illumination (AM 1.5G and 100 mW cm^{-2}). The average PCE of the devices based on **CbzBF** and **CbzBT** was significantly improved to 21.18% and 21.65%, respectively, due to the significantly enhanced FFs to 82.00% and 82.71%, and V_{oc} to 1.08 V and 1.09 V, respectively (Table 1, Fig. 4b, c and S15†). Notably, the champion PCE of the devices based on **CbzBT** was as high as 22.08% without using any additive and top surface passivation treatment, with an impressively high FF of 84.20%. The significantly enhanced FF should be benefited from the enhanced SAM intermolecular π–π interactions promoting more ordered assembly, increased molecular dipoles enabling better ITO WF regulation, and introduced Lewis basic heteroatoms passivating the buried interface. Moreover, the hole-only devices with an architecture of ITO/SAM/perovskite/MoO$_3$/Ag were fabricated for space charge-limited current (SCLC) measurements. The turning point of the ohmic region and trap-filling region of the curve revealed the trap-filled limit voltage (V_{TFL}), which were determined to be 0.873 V, 0.607 and 0.597 V for **CbzPh**-, **CbzBF**- and **CbzBT**-based devices, respectively (Fig. S16†). The lower V_{TFL} showed the lower trap density of devices based on **CbzBF** and **CbzBT** as the trap density is directly proportional to the V_{TFL}. The dark current and light intensity-dependent V_{oc} values of PSCs based on **CbzPh**-, **CbzBF**-, and **CbzBT**-modified substrates were measured (Fig. S16†). The **CbzBT**-based device shows the smallest dark current and the highest ideality factor, both of which indicate that a densely packed **CbzBT** monolayer could
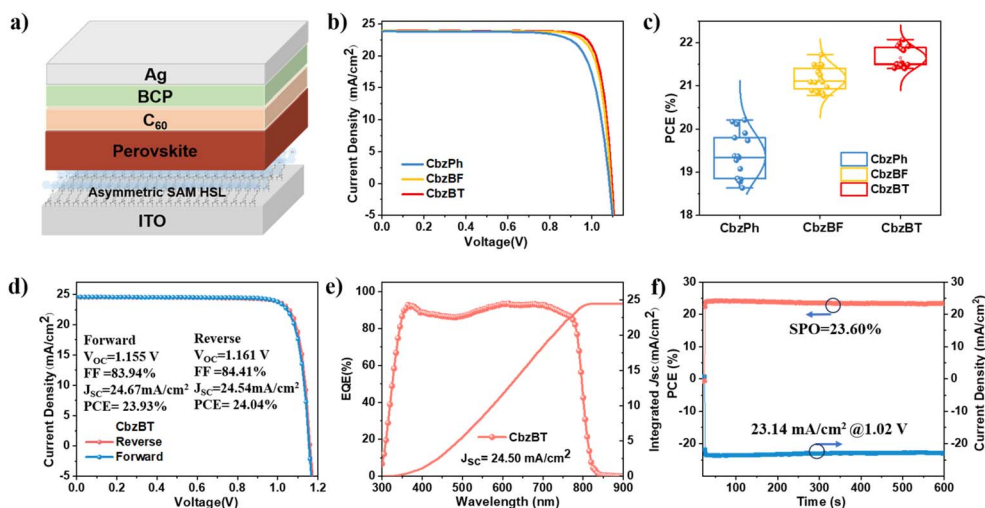

Fig. 4 (a) Device architecture of the inverted PSCs; (b) current density–voltage (J–V) characteristics; (c) box plots of the PCEs of the PSCs employing SAM-modified substrates of **CbzPh**, **CbzBF** and **CbzBT**; (d)–(f) device characteristics of (d) J–V sweeps, (e) EQE and (f) stabilized power output (SPO) of the champion device employing the **CbzBT** HSL.

Table 1 Detailed photovoltaic parameters of PSCs based on **CbzPh**, **CbzBF** and **CbzBT**. Average data were obtained from 16 cells

HSL	V_{OC} (V)	J_{SC} (mA cm^{-2})	FF (%)	PCE (%)
CbzPh	1.08	23.80	78.42	20.22
	1.06 ± 0.02	23.58 ± 0.56	76.56 ± 1.27	19.36 ± 0.54
CbzBF	1.09	24.00	83.04	21.72
	1.08 ± 0.01	23.78 ± 0.29	82.00 ± 0.55	21.18 ± 0.28
CbzBT	1.10	23.93	84.20	22.08
	1.09 ± 0.01	23.91 ± 0.22	82.71 ± 0.84	21.65 ± 0.23

effectively reduce current leakage and interfacial recombination to improve the V_{oc}, FF and stability of the corresponding PSCs.

To further understand how the interfacial properties of these SAMs as HSLs affect the charge transfer dynamics, steady-state photoluminescence (PL) (Fig. 3c) and time-resolved PL (TRPL) spectra (Fig. 3d) of perovskite on top of SAM-modified substrates were recorded to evaluate the hole extraction capability of SAMs. The PL intensity and TRPL decay traces of perovskite layers grown on **CbzBF** and **CbzBT** are significantly enhanced compared with that grown on **CbzPh** (Table S4†), reaffirming the reduced defects and suppressed non-radiative recombination at the interface after introducing the oxygen and sulfur heteroatom-containing SAMs and the more ordered assembly of SAMs. They synergistically enhanced the hole extraction capability of **CbzBF** and **CbzBT**. Between them, the S atom has higher binding energy with PbI$_2$; therefore **CbzBT** should have stronger intermolecular interaction, resulting in higher PL intensity and extended PL lifetime in the **CbzBT**-supported perovskite film.

To fully exploit the potential of the **CbzBT** HSL, top surface passivation and light management adopting anti-reflection coating were also applied.[52] The champion **CbzBT**-based device could achieve a PCE of 24.04% (V_{OC} = 1.16 V, J_{SC} = 24.54 mA cm^{-2}, and FF = 84.41%) (Fig. 4d), demonstrating the **CbzBT** HSL's great potential for inverted PSCs. To ensure the data reliability, the external quantum efficiency (EQE) of the device was also measured to calibrate the cell J_{SC} (Fig. 4e). The integrated photocurrent (24.50 mA cm^{-2}) of the champion device matches well with the value obtained from the J–V measurement. The stability of the champion cell was further assessed by tracking the stabilized power output at bias corresponding to the maximum power point (MPP) under continuous AM 1.5G illumination (Fig. 4f). A stabilized PCE of 23.60% was retrieved, which agrees well with the values from the J–V sweeps.

Since the SAM contains a flexible alkyl linker, there are concerns about potential efficiency degradation caused by the SAM's thermal motion at high temperatures. Therefore, the thermal stability of **CbzPh**-, **CbzBF**-, and **CbzBT**-based PSCs was also evaluated under an annealing temperature of 65 °C in a N$_2$-filled glove box. The devices based on **CbzBF** and **CbzBT** HSLs exhibited better thermal stability than those based on **CbzPh**, retaining 98.9% and 98.2% of their original PCE, respectively, under continuous heating for more than 700 h, which are higher than that of **CbzPh** based devices (93.3%) (Fig. S17†). The enhanced intermolecular interaction and denser assembly caused by the conjugation extension, as well as the introduced defect-passivating Lewis basic heteroatoms, synergistically enhance the stability.

Conclusions

In summary, we report two novel asymmetric SAM molecules designed by substituting the fused benzene ring on **CbzPh** with benzofuran and benzothiophene, namely **CbzBF** and **CbzBT**, to induce asymmetric conjugation extension and incorporation of lone-pair-rich, Lewis-basic oxygen and sulfur atoms for efficient hole extraction and buried interface passivation. The advantages of **CbzBF** and **CbzBT** in tuning ITO WF, optimizing perovskite crystallization, and passivating PbI$_2$ defects are demonstrated by spectroscopic and interfacial characterization. As a result, the champion device of inverted PSCs employing **CbzBT** as the HSL could achieve an impressive PCE of 24.04% along with a remarkable FF of 84.41% and improved device stability. Moreover, this work demonstrates the feasibility of introducing passivating groups into high-performance SAM molecules, and insights gained from this molecular design strategy will help accelerate the development of new multifunctional SAM HSLs for more efficient PSCs.

Data availability

The related experimental data are provided in the ESI.†

Author contributions

W. J. conceived the project and synthesized SAM molecules, which was supervised by A. K. Y. J., M. L. conducted PSC devices and interfacial characterization including XPS, SEM, PL and TRPL with the assistance of Y. L. W. J. and F. R. L. wrote the manuscript, and all authors participated in the data analysis and discussions.

Conflicts of interest

There are no conflicts to declare.

Acknowledgements

References

1 J. Park, J. Kim, H. S. Yun, M. J. Paik, E. Noh, H. J. Mun, M. G. Kim, T. J. Shin and S. I. Seok, Controlled growth of perovskite layers with volatile alkylammonium chlorides, *Nature*, 2023, **616**, 724–730.

2 X. Wu, B. Li, Z. Zhu, C. C. Chueh and A. K. Jen, Designs from single junctions, heterojunctions to multijunctions for high-performance perovskite solar cells, *Chem. Soc. Rev.*, 2021, **50**, 13090–13128.

3 S. Wu, Z. Chen, H.-L. Yip and A. K. Y. Jen, The evolution and future of metal halide perovskite-based optoelectronic devices, *Matter*, 2021, **4**, 3814–3834.

4 N. J. Jeon, J. H. Noh, W. S. Yang, Y. C. Kim, S. Ryu, J. Seo and S. I. Seok, Compositional engineering of perovskite materials for high-performance solar cells, *Nature*, 2015, **517**, 476–480.

5 T. Matsui, T. Yamamoto, T. Nishihara, R. Morisawa, T. Yokoyama, T. Sekiguchi and T. Negami, Compositional Engineering for Thermally Stable, Highly Efficient Perovskite Solar Cells Exceeding 20% Power Conversion Efficiency with 85 degrees C/85% 1000 h Stability, *Adv. Mater.*, 2019, **31**, e1806823.

6 F. Li, X. Deng, Z. Shi, S. Wu, Z. Zeng, D. Wang, Y. Li, F. Qi, Z. Zhang, Z. Yang, S.-H. Jang, F. R. Lin, S. W. Tsang, X.-K. Chen and A. K. Y. Jen, Hydrogen-bond-bridged intermediate for perovskite solar cells with enhanced efficiency and stability, *Nat. Photonics*, 2023, **17**, 478–484.

7 L. Bi, Q. Fu, Z. Zeng, Y. Wang, F. R. Lin, Y. Cheng, H. L. Yip, S. W. Tsang and A. K. Jen, Deciphering the Roles of MA-Based Volatile Additives for alpha-FAPbI(3) to Enable Efficient Inverted Perovskite Solar Cells, *J. Am. Chem. Soc.*, 2023, **145**, 5920–5929.

8 S. Shan, C. Xu, H. Wu, B. Niu, W. Fu, L. Zuo and H. Chen, Manipulating the Crystallization and Phase Transition for High-Performance CsPbI2Br Solar Cells, *Adv. Energy Mater.*, 2022, **13**, 2203682.

9 Y. Huang, K. Yan, B. Niu, Z. Chen, E. Gu, H. Liu, B. Yan, J. Yao, H. Zhu, H. Chen and C.-Z. Li, Finite perovskite hierarchical structures via ligand confinement leading to efficient inverted perovskite solar cells, *Energy Environ. Sci.*, 2023, **16**, 557–564.

10 P. Shi, Y. Ding, B. Ding, Q. Xing, T. Kodalle, C. M. Sutter-Fella, I. Yavuz, C. Yao, W. Fan, J. Xu, Y. Tian, D. Gu, K. Zhao, S. Tan, X. Zhang, L. Yao, P. J. Dyson, J. L. Slack, D. Yang, J. Xue, M. K. Nazeeruddin, Y. Yang and R. Wang, Oriented nucleation in formamidinium perovskite for photovoltaics, *Nature*, 2023, **620**, 323–327.

11 J. Xia, M. Sohail and M. K. Nazeeruddin, Efficient and Stable Perovskite Solar Cells by Tailoring of Interfaces, *Adv. Mater.*, 2023, **35**, e2211324.

12 S. Zhang, F. Ye, X. Wang, R. Chen, H. Zhang, L. Zhan, X. Jiang, Y. Li, X. Ji, S. Liu, M. Yu, F. Yu, Y. Zhang, R. Wu, Z. Liu, Z. Ning, D. Neher, L. Han, Y. Lin, H. Tian, W. Chen, M. Stolterfoht, L. Zhang, W. H. Zhu and Y. Wu, Minimizing buried interfacial defects for efficient inverted perovskite solar cells, *Science*, 2023, **380**, 404–409.

13 F. Li and A. K. Y. Jen, Interface Engineering in Solution-Processed Thin-Film Solar Cells, *Acc. Mater. Res.*, 2022, **3**, 272–282.

14 Y. Zhou, L. M. Herz, A. K. Y. Jen and M. Saliba, Advances and challenges in understanding the microscopic structure–property–performance relationship in perovskite solar cells, *Nat. Energy*, 2022, **7**, 794–807.

15 B. Niu, H. Liu, Y. Huang, E. Gu, M. Yan, Z. Shen, K. Yan, B. Yan, J. Yao, Y. Fang, H. Chen and C. Z. Li, Multifunctional Hybrid Interfacial Layers for High-Performance Inverted Perovskite Solar Cells, *Adv. Mater.*, 2023, **35**, e2212258.

16 M. Kim, J. N. Hohman, Y. Cao, K. N. Houk, H. Ma, A. K. Jen and P. S. Weiss, Creating favorable geometries for directing organic photoreactions in alkanethiolate monolayers, *Science*, 2011, **331**, 1312–1315.

17 O. Acton, D. Hutchins, L. Arnadottir, T. Weidner, N. Cernetic, G. G. Ting, T. W. Kim, D. G. Castner, H. Ma and A. K. Jen, Spin-cast and patterned organophosphonate self-assembled monolayer dielectrics on metal-oxide-activated Si, *Adv. Mater.*, 2011, **23**, 1899–1902.

18 H.-L. Yip, S. K. Hau, N. S. Baek, H. Ma and A. K. Y. Jen, Polymer Solar Cells That Use Self-Assembled-Monolayer-Modified ZnO/Metals as Cathodes, *Adv. Mater.*, 2008, **20**, 2376–2382.

19 A. Magomedov, A. Al-Ashouri, E. Kasparavičius, S. Strazdaite, G. Niaura, M. Jošt, T. Malinauskas, S. Albrecht and V. Getautis, Self-Assembled Hole Transporting Monolayer for Highly Efficient Perovskite Solar Cells, *Adv. Energy Mater.*, 2018, **8**, 1801892.

20 A. Al-Ashouri, A. Magomedov, M. Roß, M. Jošt, M. Talaikis, G. Chistiakova, T. Bertram, J. A. Márquez, E. Köhnen, E. Kasparavičius, S. Levcenco, L. Gil-Escrig, C. J. Hages, R. Schlatmann, B. Rech, T. Malinauskas, T. Unold, C. A. Kaufmann, L. Korte, G. Niaura, V. Getautis and S. Albrecht, Conformal monolayer contacts with lossless interfaces for perovskite single junction and monolithic tandem solar cells, *Energy Environ. Sci.*, 2019, **12**, 3356–3369.

21 J. Y. Lee, S. Y. Kim and H. J. Yoon, Small Molecule Approach to Passivate Undercoordinated Ions in Perovskite Light Emitting Diodes: Progress and Challenges, *Adv. Opt. Mater.*, 2021, **10**, 2101361.

22 K. Rakstys, C. Igci and M. K. Nazeeruddin, Efficiency vs. stability: dopant-free hole transporting materials towards stabilized perovskite solar cells, *Chem. Sci.*, 2019, **10**, 6748–6769.

23 E. Li, C. Liu, H. Lin, X. Xu, S. Liu, S. Zhang, M. Yu, X. M. Cao, Y. Wu and W. H. Zhu, Bonding Strength Regulates Anchoring-Based Self-Assembly Monolayers for Efficient and Stable Perovskite Solar Cells, *Adv. Funct. Mater.*, 2021, **31**, 2103847.

24 R. Azmi, E. Ugur, A. Seitkhan, F. Aljamaan, A. S. Subbiah, J. Liu, G. T. Harrison, M. I. Nugraha, M. K. Eswaran, M. Babics, Y. Chen, F. Xu, T. G. Allen, A. U. Rehman, C. L. Wang, T. D. Anthopoulos, U. Schwingenschlogl, M. De Bastiani, E. Aydin and S. De Wolf, Damp heat-stable

perovskite solar cells with tailored-dimensionality 2D/3D heterojunctions, *Science*, 2022, **376**, 73–77.

25 E. Li, E. Bi, Y. Wu, W. Zhang, L. Li, H. Chen, L. Han, H. Tian and W. H. Zhu, Synergistic Coassembly of Highly Wettable and Uniform Hole-Extraction Monolayers for Scaling-up Perovskite Solar Cells, *Adv. Funct. Mater.*, 2019, **30**, 1909509.

26 A. Ullah, K. H. Park, H. D. Nguyen, Y. Siddique, S. F. A. Shah, H. Tran, S. Park, S. I. Lee, K. K. Lee, C. H. Han, K. Kim, S. Ahn, I. Jeong, Y. S. Park and S. Hong, Novel Phenothiazine-Based Self-Assembled Monolayer as a Hole Selective Contact for Highly Efficient and Stable p-i-n Perovskite Solar Cells, *Adv. Energy Mater.*, 2021, **12**, 2103175.

27 W. Jiang, F. Li, M. Li, F. Qi, F. R. Lin and A. K. Jen, pi-Expanded Carbazoles as Hole-Selective Self-Assembled Monolayers for High-Performance Perovskite Solar Cells, *Angew. Chem., Int. Ed.*, 2022, **61**, e202213560.

28 M. Liu, L. Bi, W. Jiang, Z. Zeng, S. W. Tsang, F. R. Lin and A. K. Jen, Compact Hole-selective Self-assembled Monolayers Enabled by Disassembling Micelles in Solution for Efficient Perovskite Solar Cells, *Adv. Mater.*, 2023, e2304415.

29 M. A. Truong, T. Funasaki, L. Ueberricke, W. Nojo, R. Murdey, T. Yamada, S. Hu, A. Akatsuka, N. Sekiguchi, S. Hira, L. Xie, T. Nakamura, N. Shioya, D. Kan, Y. Tsuji, S. Iikubo, H. Yoshida, Y. Shimakawa, T. Hasegawa, Y. Kanemitsu, T. Suzuki and A. Wakamiya, Tripodal Triazatruxene Derivative as a Face-On Oriented Hole-Collecting Monolayer for Efficient and Stable Inverted Perovskite Solar Cells, *J. Am. Chem. Soc.*, 2023, **145**, 7528–7539.

30 I. Lange, S. Reiter, M. Pätzel, A. Zykov, A. Nefedov, J. Hildebrandt, S. Hecht, S. Kowarik, C. Wöll, G. Heimel and D. Neher, Tuning the Work Function of Polar Zinc Oxide Surfaces using Modified Phosphonic Acid Self-Assembled Monolayers, *Adv. Funct. Mater.*, 2014, **24**, 7014–7024.

31 C. M. Hung, C. L. Mai, C. C. Wu, B. H. Chen, C. H. Lu, C. C. Chu, M. C. Wang, S. D. Yang, H. C. Chen, C. Y. Yeh and P. T. Chou, Self-Assembled Monolayers of Bi-Functionalized Porphyrins: A Novel Class of Hole-Layer-Coordinating Perovskites and Indium Tin Oxide in Inverted Solar Cells, *Angew. Chem., Int. Ed.*, 2023, e202309831.

32 H. Liu, K. Yan, J. Rao, Z. Chen, B. Niu, Y. Huang, H. Ju, B. Yan, J. Yao, H. Zhu, H. Chen and C. Z. Li, Self-Assembled Donor-Acceptor Dyad Molecules Stabilize the Heterojunction of Inverted Perovskite Solar Cells and Modules, *ACS Appl. Mater. Interfaces*, 2022, **14**, 6794–6800.

33 X. Deng, F. Qi, F. Li, S. Wu, F. R. Lin, Z. Zhang, Z. Guan, Z. Yang, C. S. Lee and A. K. Jen, Co-assembled Monolayers as Hole-Selective Contact for High-Performance Inverted Perovskite Solar Cells with Optimized Recombination Loss and Long-Term Stability, *Angew. Chem., Int. Ed.*, 2022, **61**, e202203088.

34 Y. Yao, C. Cheng, C. Zhang, H. Hu, K. Wang and S. De Wolf, Organic Hole-Transport Layers for Efficient, Stable, and

35 J. Xia, Y. Zhang, M. Cavazzini, S. Orlandi, B. Ding, H. Kanda, N. Klipfel, X. X. Gao, Q. Ul Ain, V. Jankauskas, R. Rakstys, R. Hu, Z. Qiu, A. M. Asiri, H. Kim, P. J. Dyson, G. Pozzi and M. Khaja Nazeeruddin, Asymmetrically Substituted 10H,10'H-9,9'-Spirobi[acridine] Derivatives as Hole-Transporting Materials for Perovskite Solar Cells, *Angew. Chem., Int. Ed.*, 2022, **61**, e202212891.

36 W. Jiang, Z. Liu, D. Zhu, W. Zheng, L. Chen, X. Zhang, G. Zhang, Y. Yi, L. Jiang and D. Zhang, New Synthetic Approaches to N-Aryl and pi-Expanded Diketopyrrolopyrroles as New Building Blocks for Organic Optoelectronic Materials, *Angew. Chem., Int. Ed.*, 2021, **60**, 10700–10708.

37 W. Wang, X. Liu, J. Wang, C. Chen, J. Yu, D. Zhao and W. Tang, Versatile Self-Assembled Molecule Enables High-Efficiency Wide-Bandgap Perovskite Solar Cells and Organic Solar Cells, *Adv. Energy Mater.*, 2023, **13**, 2300694.

38 C. Li, X. Wang, E. Bi, F. Jiang, S. M. Park, Y. Li, L. Chen, Z. Wang, L. Zeng, H. Chen, Y. Liu, C. R. Grice, A. Abudulimu, J. Chung, Y. Xian, T. Zhu, H. Lai, B. Chen, R. J. Ellingson, F. Fu, D. S. Ginger, Z. Song, E. H. Sargent and Y. Yan, Rational design of Lewis base molecules for stable and efficient inverted perovskite solar cells, *Science*, 2023, **379**, 690–694.

39 O. Acton, M. Dubey, T. Weidner, K. M. O'Malley, T.-W. Kim, G. G. Ting, D. Hutchins, J. E. Baio, T. C. Lovejoy, A. H. Gage, D. G. Castner, H. Ma and A. K. Y. Jen, Simultaneous Modification of Bottom-Contact Electrode and Dielectric Surfaces for Organic Thin-Film Transistors Through Single-Component Spin-Cast Monolayers, *Adv. Funct. Mater.*, 2011, **21**, 1476–1488.

40 S. Y. Lee, Y. Choi, E. Ito, M. Hara, H. Lee and J. Noh, Growth, solvent effects, and thermal desorption behavior of octylthiocyanate self-assembled monolayers on Au(111), *Phys. Chem. Chem. Phys.*, 2013, **15**, 3609–3617.

41 I. Levine, A. Al-Ashouri, A. Musiienko, H. Hempel, A. Magomedov, A. Drevilkauskaite, V. Getautis, D. Menzel, K. Hinrichs, T. Unold, S. Albrecht and T. Dittrich, Charge transfer rates and electron trapping at buried interfaces of perovskite solar cells, *Joule*, 2021, **5**, 2915–2933.

42 C.-H. Chen, Y.-T. Hsu, B.-C. Wang, C.-L. Chung and C.-P. Chen, Thienoisoindigo-Based Dopant-Free Hole Transporting Material for Efficient p–i–n Perovskite Solar Cells with the Grain Size in Micrometer Scale, *J. Phys. Chem. C*, 2018, **123**, 1602–1609.

43 C. Bi, Q. Wang, Y. Shao, Y. Yuan, Z. Xiao and J. Huang, Non-wetting surface-driven high-aspect-ratio crystalline grain growth for efficient hybrid perovskite solar cells, *Nat. Commun.*, 2015, **6**, 7747.

44 S. Y. Kim, H. Kang, K. Chang and H. J. Yoon, Case Studies on Structure-Property Relations in Perovskite Light-Emitting Diodes via Interfacial Engineering with Self-Assembled Monolayers, *ACS Appl. Mater. Interfaces*, 2021, **13**, 31236–31247.

45 Y. Deng, X. Zheng, Y. Bai, Q. Wang, J. Zhao and J. Huang, Surfactant-controlled ink drying enables high-speed deposition of perovskite films for efficient photovoltaic modules, *Nat. Energy*, 2018, **3**, 560–566.

46 J. A. Bardecker, H. Ma, T. Kim, F. Huang, M. S. Liu, Y.-J. Cheng, G. Ting and A. K. Y. Jen, Self-assembled Electroactive Phosphonic Acids on ITO: Maximizing Hole-Injection in Polymer Light-Emitting Diodes, *Adv. Funct. Mater.*, 2008, **18**, 3964–3971.

47 B. Roose, K. Dey, Y. H. Chiang, R. H. Friend and S. D. Stranks, Critical Assessment of the Use of Excess Lead Iodide in Lead Halide Perovskite Solar Cells, *J. Phys. Chem. Lett.*, 2020, **11**, 6505–6512.

48 V. Sarritzu, N. Sestu, D. Marongiu, X. Chang, S. Masi, A. Rizzo, S. Colella, F. Quochi, M. Saba, A. Mura and G. Bongiovanni, Optical determination of Shockley-Read-Hall and interface recombination currents in hybrid perovskites, *Sci. Rep.*, 2017, **7**, 44629.

49 C. M. Wolff, P. Caprioglio, M. Stolterfoht and D. Neher, Nonradiative Recombination in Perovskite Solar Cells: The Role of Interfaces, *Adv. Mater.*, 2019, **31**, e1902762.

50 C. Fei, N. Li, M. Wang, X. Wang, H. Gu, B. Chen, Z. Zhang, Z. Ni, H. Jiao, W. Xu, Z. Shi, Y. Yan and J. Huang, Lead-chelating hole-transport layers for efficient and stable perovskite minimodules, *Science*, 2023, **380**, 823–829.

51 X. Ji, L. Bi, Q. Fu, B. Li, J. Wang, S. Y. Jeong, K. Feng, S. Ma, Q. Liao, F. R. Lin, H. Y. Woo, L. Lu, A. K. Jen and X. Guo, Target Therapy for Buried Interface Enables Stable Perovskite Solar Cells with 25.05% Efficiency, *Adv. Mater.*, 2023, e2303665.

52 F. Li, X. Deng, F. Qi, Z. Li, D. Liu, D. Shen, M. Qin, S. Wu, F. Lin, S. H. Jang, J. Zhang, X. Lu, D. Lei, C. S. Lee, Z. Zhu and A. K. Jen, Regulating Surface Termination for Efficient Inverted Perovskite Solar Cells with Greater Than 23% Efficiency, *J. Am. Chem. Soc.*, 2020, **142**, 20134–20142.